J. Wind Eng. Ind. Aerodyn. 107–108 (2012) 285–298

Contents lists available at SciVerse ScienceDirect

Journal of Wind Engineering and Industrial Aerodynamics

journal homepage: www.elsevier.com/locate/jweia

Fragility curves for building envelope components subject to windborne debris impact

A.H. Herbin, M. Barbato *

Department of Civil and Environmental Engineering, Louisiana State University, Patrick F. Taylor Hall, Baton Rouge, LA 70803, USA

ARTICLE INFO

Article history:
Received 24 October 2011
Received in revised form
7 May 2012
Accepted 28 May 2012
Available online 20 June 2012

Keywords:
Performance-based engineering
Windborne debris
Finite element method
Building envelope components
Fragility curves

ABSTRACT

This paper presents a methodology for developing windborne debris (WBD) impact fragility curves for building envelope components (BECs) by using stochastic finite element (FE) models. These fragility curves provide the probabilistic description of the impact resistance of BECs subject to an impact event described by an appropriate intensity measure (*IM*). Accurate fragility curves are essential in the development of a general probabilistic performance-based engineering framework for mitigation of WBD impact hazard.

Monte Carlo simulation is used in combination with the FE method to propagate uncertainties in the BEC's model parameters and WBD impact location. As an application example, the fragility curves relative to different damage states are derived for aluminum storm shutters subjected to WBD impact. It is found that (1) the missile kinetic energy at impact is a sufficient *IM* for BECs with ductile behavior subjected to WBD impact, and (2) the performance of storm panels in terms of penetration of WBDs is critically dependent on the details of the panels' installation.

1. Introduction

The threat of natural disasters is a significant concern to society. Hurricanes, for example, frequently cause severe damage to structural and infrastructural systems in the United States of America (NSB, 2007; Pielke et al., 2008) and worldwide (Kentang, 2000; Stewart, 2003). Severe tropical storms are often the cause of structural damage and loss of life. Therefore, it is important for engineers to design structures that can adequately accommodate the extreme loading produced by hurricane events (e.g., due to wind pressure, flooding, and/or windborne debris (WBD) impact) with an optimal use of available resources. Over the past few decades, significant advances have been achieved in risk assessment and mitigation for structures subjected to hurricane hazard (Li and Ellingwood, 2006; Holmes, 2008, 2010). The advancement of structural reliability analysis and the development of probabilistic performance-based techniques have been integral to these advances. Structural reliability techniques allow the rigorous consideration of uncertainties inherent in engineering problems and are used for the calibration of design codes (Nowak, 1999; Abu-Farsakh et al., 2010; Kwon et al., 2011). Probabilistic performance-based methods are extensively developed in the field of earthquake engineering (Cornell and Krawinkler, 2000; Porter, 2003). Similar methodologies, based on a performance-based engineering (PBE) approach, are currently being developed in other civil engineering subfields, including wind, fire, and blast engineering (Hamburger and Whittaker, 2003; Augusti and Ciampoli, 2006; Rini and Lamont, 2008; Ciampoli et al., 2009; Petrini, 2009).

PBE targets the achievement of specified levels of performance for a structural system rather than following a prescriptive approach over an entire spectrum of design problems (based on general equations and calibrated coefficients, the use of which is considered sufficient to satisfy some implicitly assumed levels of performance). The aim of PBE is to ensure a sufficiently small probability, over the design life of the structure, that the damage to a structure will exceed any limit states describing failure (e.g., physical failure, member buckling), serviceability (e.g., maximum deformation, occupant comfort), and/or other performance measures (Bertero and Vitelmo, 2002). In PBE, the response of a structure is described by engineering demand parameters (*EDP*s) (e.g., maximum deformation, maximum displacement, maximum force applied on a member) and is evaluated with respect to different levels of an intensity measure (*IM*). In earthquake engineering, several scalar (e.g., peak ground acceleration (Bertero and Vitelmo, 2002), first-mode spectral acceleration (Luco and Cornell, 2007)) and vector *IM*s (Baker and Cornell, 2005, 2008; Vamvatsikos and Cornell, 2005) have been identified and employed. In hurricane engineering, physical quantities

* Corresponding author. Tel.: +1 225 578 8719; fax: +1 225 578 4945.
E-mail addresses: aherbi1@tigers.lsu.edu (A.H. Herbin), mbarbato@lsu.edu (M. Barbato).

0167-6105/$ - see front matter © 2012 Elsevier Ltd. All rights reserved.
http://dx.doi.org/10.1016/j.jweia.2012.05.005

related to mean wind speed are good candidates for use as efficient and sufficient *IM*s (Petrini, 2009).

Performance is determined by comparing the response of the structure to appropriate damage measures (*DM*s), which are used to describe physical states of damage (Porter, 2003). The PBE methodology can also provide an estimate of structural risk by determining the probability of exceeding a given value of a decision variable (*DV*) which corresponds to a specified level of performance (Barbato et al., 2011). A *DV* is defined as a measurable quantity that represents the cost and/or benefit (e.g., monetary losses, loss of lives, downtime, and/or other factors) for the owner, the users, and/or the society resulting from the structure under consideration (Porter, 2003). *DV*s for several design options can be compared in a PBE assessment analysis to guide the rational selection of a final design (Barbato et al., 2011).

A critical feature of probabilistic PBE methods is the explicit consideration of uncertainties. Uncertainties can be classified into two different categories, i.e., inherent randomness (due to natural variability of physical, geometrical, and mechanical properties) and epistemic uncertainties (due to lack of knowledge, imprecise modeling, and limited statistical information) (Lupoi et al., 2006). Inherent randomness is virtually irreducible since it is an inevitability of nature. In contrast, epistemic uncertainties can be reduced, e.g., by implementing more accurate and realistic models. There is a great need to develop a probabilistic PBE methodology in the field of hurricane engineering since the effects of a hurricane on the built and natural environment are characterized by significant uncertainties and cannot be predicted using only deterministic models.

Among the tools developed in probabilistic PBE, significant research interest has been focused on the construction of fragility curves (Gardoni et al., 2002; Lupoi et al., 2006; Brandenberg et al., 2011). Fragility curves are the cumulative distribution functions (CDFs) of the structural capacity with respect to a specific limit-state, usually corresponding to a physical damage state for the structural system under consideration (Mackie and Stojadinovic, 2004). In hurricane engineering, only limited research has been devoted to fragility analysis (Gurley et al., 2005a,b; Li and Ellingwood, 2006; FEMA, 2007). Thus, there is a need to develop fragility curves for structural and non-structural components of buildings. It has been shown that the building envelope is the building component most susceptible to damage during a hurricane (Li and Ellingwood, 2006). The building envelope consists of non-structural components such as non-load-bearing walls, windows, doors, and roofing. When the building envelope is compromised, the structure is subjected to a much higher risk of damage due to increased internal wind pressure and water penetration from rain and flooding (Li and Ellingwood, 2006; Lopez et al. 2011). In hurricane prone regions, protection for the most critical elements in the building envelope is often installed in the form of shutters, plywood, and other types of movable reinforcement.

Substantial research has focused on WBD hazard in residential settings and performance of building envelope components (BECs) subject to WBD impact loading. Earlier studies focused on practical design approaches (Minor et al., 1978), on the deterministic description of the flight characteristics of different WBD (Tachikawa, 1983, 1988), and on the resistance of different materials to WBD impact (McDonald, 1990). In the recent past and particularly after the extensive damage to glazing elements produced by Hurricane Andrew (NAHB, 1993), an increased attention was given to risk analysis (Twisdale et al., 1996) and damage analysis (NAHB, 2002; Willis et al., 2002). This new interest led to improved standardized tests for WBD impact resistance of BECs (ASTM, 2005a,b) and probability-based damage models for BECs subject to WBD impact hazard (Pinelli et al., 2004; Gurley et al., 2006; FEMA, 2007).

More recently, significant research has been devoted to the study of WBD flight trajectories and speeds (Lin et al., 2006, 2007; Martinez-Vazquez et al., 2010; Kordi et al., 2010; Kakimpa et al., 2010; Scarabino and Giacopinelli, 2010), on WBD risk analysis (Holmes, 2008, 2010; Lin and Vanmarcke, 2010; Lin et al., 2010), and on the vulnerability of BECs (Masters et al., 2010; Fernandez et al., 2010). It is noted here that only scarce information is available regarding the fragility of BECs with ductile behavior (Borges et al., 2009; Fernandez et al., 2010).

The objective of this research is to propose a methodology for developing the fragility curves corresponding to representative damage states for BECs and BEC protection systems subjected to WBD impact loading. This methodology is based on the combination of finite element (FE) analysis and Monte Carlo simulation (MCS) (Liu, 2001), and is integrated into a general probabilistic PBE framework. The fragility curves corresponding to different damage states are derived for a storm panel representative of BECs with ductile behavior. Appropriate *IM*s, *EDP*s, and *DM*s for BECs with ductile behavior are also identified.

2. Methodology

The methodology adopted in this paper is derived from the performance-based earthquake engineering (PBEE) framework developed by the Pacific Earthquake Engineering Research Center (PEER). The PEER PBEE method is a general and widely accepted example of probabilistic PBE based on the total probability theorem (Cornell and Krawinkler, 2000; Porter, 2003; Barbato et al., 2011). The PEER PBEE framework computes the mean annual frequency of exceeding a specific level of a *DV*, $g[DV]$, as:

$$\begin{aligned} g[DV] &= \iiint G[DV|DM] \times p[DM|EDP] \times p[EDP|IM] \\ &\quad \times \left|\frac{\mathrm{d}g[IM]}{\mathrm{d}IM}\right| \times \mathrm{d}IM \times \mathrm{d}EDP \times \mathrm{d}DM \\ &= \iiint G[DV|DM] \times |\mathrm{d}G[DM|EDP]| \times |\mathrm{d}G[EDP|IM]| \times |\mathrm{d}g[IM]| \end{aligned} \tag{1}$$

in which $G[A|B]$ = complementary cumulative distribution function (CDF) of random variable A conditional on a specified value of random variable B, $p[A|B]$ = probability density function (PDF) of random variable A conditional on a specified value of random variable B, and $g[A]$ = mean annual frequency of variable A outcrossing a specified value. In Eq. (1), the two equivalent forms are obtained by using the relation $|\mathrm{d}G[A|B]| = p[A|B]\cdot \mathrm{d}A$. The analysis is decomposed into four phases that must be conducted sequentially. The parameters used in any step are chosen so that they remain independent of those from all previous steps (Barbato et al., 2011). The first phase is known as hazard analysis and consists of defining a hazard curve or hazard function, $g[IM]$, for the specific location of the structure. The hazard function defines the frequency in which different levels of intensity of the hazard considered are exceeded in a given time frame. Several studies on hurricane hazard analysis are available in the literature (Vickery and Twinsdale, 1995; Hossain et al., 1999; Vickery et al., 2006, FEMA, 2007; Vickery et al., 2009; Lin and Vanmarcke, 2010). In the second phase, referred to as structural analysis, a structural model is used to determine the PDF of the *EDP*(s) conditional to *IM*, i.e., $p[EDP|IM]$. The third phase, referred to as damage analysis, is used to determine the fragility functions that describe the probability of exceeding a specific limit state represented in the form of a *DM*, i.e., $p[DM|EDP]$. Decision variables (*DV*) related to structural damage are then considered in the loss analysis phase, yielding $p[DV|DM]$ in Eq. (1). Several studies on hurricane loss

analysis are also available in the literature (Gurley et al., 2005b, 2006; FEMA, 2007; Lin et al., 2010; Yau, 2011).

This research proposes to adapt the probabilistic PBE framework developed by PEER for earthquake engineering to hurricane engineering problems, with particular emphasis on the assessment and mitigation of WBD impact risk. A crucial component of this research is the identification of appropriate *IM*s that are sufficient and efficient (Shome et al., 1998) as well as *EDP*s and *DM*s describing the structural response parameters and damage states, respectively, that are relevant to assess the risk due to WBD impact. The focus of this paper is the development of fragility curves for BECs with ductile behavior subjected to WBD impact. Fragility curves are obtained from the following convolution integral

$$G[DM] = \int G[DM|EDP] \times |dG[EDP|IM]| \quad (2)$$

Eq. (2) involves both the structural analysis and the damage analysis components of the PBE framework.

These fragility curves are constructed using results obtained from stochastic FE models that account for inherent uncertainties in both the BECs and in the location of WBD impact. The stochastic FE approach adopted in this study consists of building a set of FE models with the parameters' values obtained from MCS. The joint PDF of these parameters is built using an appropriate model based on the available statistical information (e.g., a Nataf's model consistent with the first- and second-order statistics of the parameters (Der Kiureghian and Liu, 1986)). From the mechanical response of the FE models of the BECs subjected to WBD impact, the statistics of the relevant *EDP*s are computed and used to fit an analytical CDF to the simulation results. In the damage analysis phase, relevant damage states are identified and the statistical description of the corresponding *DM*s is obtained, based on available data and/or on engineering judgment. Finally, the statistical description of the *EDP*s and *DM*s are convolved to derive the fragility curves for the *DM*s of interest.

The methodology described here is very general and can be applied to any structural component, non-structural component, and/or system subjected to WBD impact hazard. It is clear that every different component/system will require the definition of different *IM*s and will be described by different *EDP*s and *DM*s. Compiling an exhaustive list of possible *IM*s, *EDP*s, and *DM*s is beyond the scope of this study. In this paper, the proposed methodology is illustrated for the specific problem of an aluminum storm panel (which is representative of BECs with ductile behavior) subjected to WBD impact hazard.

3. Structural modeling of BECs

3.1. Description of physical specimen

BEC protection options readily available for practical applications include different types of hurricane shutters, e.g., Bahama shutters, colonial shutters, and storm panels. This research considers corrugated aluminum hurricane panels, which are chosen over other options based on their relatively low cost and ease of installation. The geometrical schematics of this type of hurricane protection are readily available. The side dimensions of the panel are height $H=47.25$ in (120.015 cm), and width $W=14.375$ in (36.513 cm). The aluminum panels are made of 0.05″ (1.27 mm) gage 3004H34 type aluminum. A picture of the storm panel's physical specimen is shown in Fig. 1(a).

The test missiles are $2'' \times 4''$ (nominal dimensions: 5.08 cm and 10.16 cm) pieces of pine wood lumber (with actual dimensions after curing and finishing of 1.5 in (3.81 cm) and 3.5 in (8.89 cm))

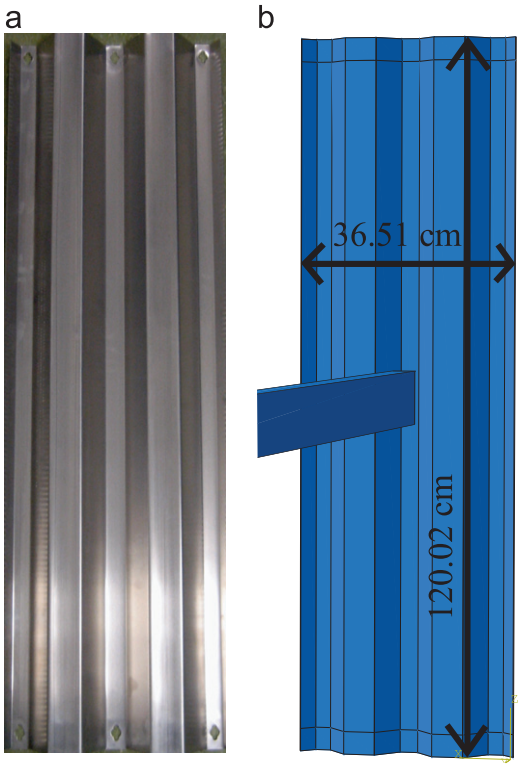

Fig. 1. Aluminum storm panel: (a) Picture of a physical specimen, and (b) ABAQUS FE model.

weighing 9, 12, and 15 pounds (corresponding to masses of 4.08, 5.44, and 6.80 kg), which represent the typical missiles recommended for use in the ASTM E1996 Standard (ASTM, 2005b). This standard specifies the minimum required performance for protective systems which are impacted during extreme wind events. According to the standard, such elements must be able to withstand the impact of a 9-pound $2'' \times 4''$ missile traveling at 90 ft/s (27.4 m/s). Thus, it is clear that the ASTM E1996 Standard requirements correspond to a prescriptive approach, which does not consider explicitly the uncertainties of WBD impact.

It is noted here that while this study focuses on the impact of $2'' \times 4''$ wooden missiles (rod-type of WBD), which are recommended in the ASTM E1996 Standard for testing the performance of storm panels, the performance-based approach proposed in this paper can be applied and should be extended to the analysis of other types of WBD as well, i.e., compact-type debris and sheet-type debris (e.g., roof shingles, roof sheathing). In fact, available literature suggests that the performance of glazing elements and protective devices for the building envelope is strongly dependent on the WBD type (NAHB, 2002; Masters et al., 2010; Fernandez et al., 2010).

3.2. Finite element modeling

The commercially available FE program ABAQUS (DSS, 2008) is employed in this research to perform the nonlinear FE dynamic impact analyses required to estimate the effects of WBD impact on the storm panel. ABAQUS is chosen for its flexibility and extensive modeling options. Within ABAQUS, a complete model can be constructed using built-in CAD capabilities. ABAQUS also provides the user with several solution algorithms and a vast database of element types. Critical features of ABAQUS pertaining to WBD impact modeling include its capabilities for dynamic

impact analysis and for nonlinear FE analysis, including both nonlinear material behavior and nonlinear geometry (DSS, 2008).

The three-dimensional geometrical representation of the two different model parts (i.e., the aluminum panel and the wood missile) is obtained by extrusion of the technical drawings of the panel's cross-section (obtained from the producer's website (AGI Group, 2006), see Fig. 2(a)) and the cross-section of a $2'' \times 4''$ lumber missile.

Each part is modeled using material constitutive models readily available in the ABAQUS library. The wood constituting the missiles is modeled as a linear elastic material, while the storm panel's aluminum is modeled using an isotropic hardening material model (similar to the material model used in Roeder and Sun (2001), in which impact of steel projectiles on aluminum/alumina laminates was studied). This modeling choice is based on the fact that isotropic hardening is generally more significant for problems involving high levels of plastic strain for a single load cycle (like the ones considered in this study) when compared to kinematic hardening effects, which can become more important in modeling the mechanical response of materials subjected to cyclic loadings with large hysteresis cycles. The parameters used to define the material constitutive models of wood and aluminum are shown in Table 1.

Once the model's individual parts are defined, they are assembled into a three-dimensional FE model using the ABAQUS CAE assembly module (see Fig. 1(b)). One of the panel's corners is located at the origin of the global coordinate system to ensure that the panel's local coordinates correspond to the model's global coordinates. This allows for easy relocation of the missile's impact point from trial to trial. The boundary conditions of the panel component are imposed in order to simulate the vertical mounting of the panel on a fixed rail system, which represents a common installation option (see Fig. 2(b)). The top and bottom edges (i.e., the shorter sides) of the panel are fixed (i.e., the nodal displacements are constrained to be equal to zero in all three coordinates) and the portions of the panel that are in direct contact with the mounting system are constrained to allow motion only in the plane of the panel. These boundary conditions correspond to the connection between the panel and the rail

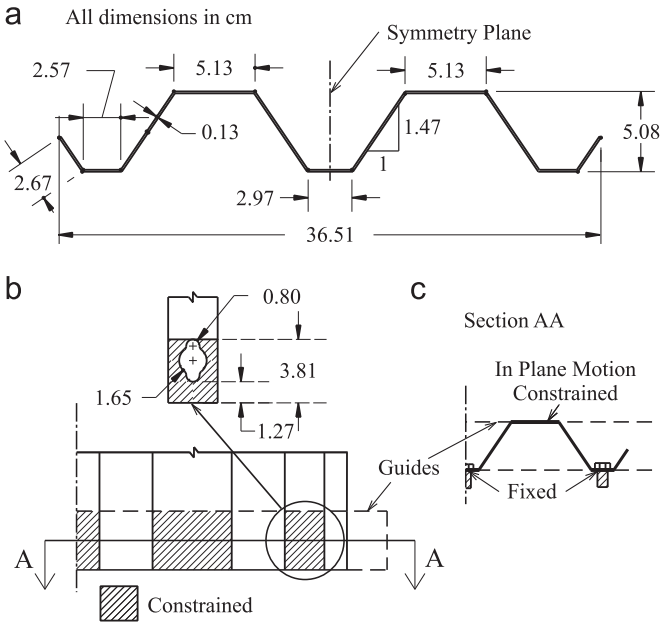

Fig. 2. Aluminum storm panel: (a) Panel cross section, (b) boundary conditions corresponding to the considered installation, and (c) details of the installation and corresponding physical constraints.

Table 1
Statistical characterization of model parameters.

Parameter	Units	Mean	COV	Distribution	Min	Max
Missile: Pine wood						
Density	kg/m^3	494.252	–	–	–	–
Young's modulus	GPa	8.963	–	–	–	–
Poisson's ratio	–	0.387	–	–	–	–
Panel: 3004H34 aluminum						
Density	kg/m^3	2720.935	–	–	–	–
Young's modulus	GPa	68.948	10	Normal	–	–
Poisson's ratio	–	0.350	–	–	–	–
Yield strength	MPa	199.948	10	Normal	–	–
Ultimate strength	MPa	241.317	10	Normal	–	–
Strain at rupture	–	0.120	–	–	–	–
Missile impact location						
X impact location	cm	–	–	Uniform	0	36.513
Y impact location	cm	–	–	Uniform	0	120.015

system which is provided through the use of bolts (see Fig. 2(c)). The left and right sides (i.e., the longer sides) of the panel are modeled as unconstrained. A predefined initial velocity field (before impact) is applied to the missile. Surface contact between the different components (i.e., the panel and the missile) is modeled using the penalty contact algorithm (DSS, 2008; Laursen, 2002). The contact surfaces in the model are taken to be the entire surface of the missile as one surface and the entire surface of the aluminum panel as the other surface. The element type used for both the panel and missile is a standard 3D hexahedral C3D8R element with linear displacement interpolation in each direction, which is available in the ABAQUS FE library. These elements incorporate hourglass control and a selectively reduced integration scheme which under-integrates volumetric strain terms and fully integrates deviatoric strain terms (DSS, 2008; Belytschko et al., 2000; Hughes, 1987). The model mass is defined by assigning to each material a mass per unit volume, the values of which are given in Table 1.

ABAQUS uses the defined density to calculate the inertia properties of the FE model using a lumped mass formulation, i.e., the total mass obtained from the volume of the FEs and the corresponding material density is concentrated in the individual nodes of each element during the dynamic FE analysis (DSS, 2008).

3.3. Dynamic finite element impact analysis

WBD impact is analyzed with ABAQUS by using the nonlinear dynamic FE analysis technique. The FE model is analyzed using the explicit central-difference direct integration scheme (DSS, 2008). WBD impact is simulated over a 0.03 s time history with an automatic time incrementation scheme, which ensures global stability of the time integration scheme. The duration of the time history is chosen so that both the peak response at impact and the vibration response after impact can be examined. Results are reported at 0.0005 s intervals, allowing for the accurate representation of the dynamic response of the panel. A FE mesh sensitivity study is performed to ensure that the FE results obtained in this study are independent of the mesh size. A mesh with FE size smaller than or equal to 0.25 in. (0.635 cm) is found to provide FE response results that are converged with respect to the FE mesh size. The FE model with mesh independent response (which is used in the remainder of this study) has a total of 19,411 elements, 38,104 nodes, and 114,312 degrees of freedom.

It is noted here that the FE model used in this study can accurately capture the time history of the deflection and plastic deformation in the storm panel and the rebounding of the missile.

However, this FE model does not explicitly represent the fracture of the metal panel, nor does it explicitly represent the plastic damage to or disintegration of the wooden missile, which is modeled using a linear elastic material constitutive model. Explicit modeling of the fracture of the metal panel would require the use of a damage parameter and an automatic removal technique of the regions in the FE model with excessive damage (Hooputra et al., 2004). Such a modeling approach, although rigorous, would require experimental information on the panel's material behavior which is not currently available. In this study, the fracture of the metal panel is verified a-posteriori, based on the maximum plastic strain in the panel. The possible damage or fragmentation of the wooden missile is also checked a-posteriori, based on a comparison between the maximum values of the principal stress components in the missile computed over the entire time history analysis, and the strength of pine wood under saturated conditions (Green and Kretschmann, 1994).

3.4. Modeling of parameter uncertainty

The FE models employed to estimate the *EDP*s' statistics are built using the sampled values of the model parameters obtained through MCS. This study considers the uncertainties in both the material properties of the aluminum panels and the location of the WBD impact. The modulus of elasticity, yield stress, and ultimate strength of aluminum are modeled as normally distributed random variables, while the aluminum Poisson's ratio and strain at rupture, as well as the pine wood mechanical properties and the material densities of both aluminum and wood are modeled as deterministic quantities. The effects of space variability of these uncertain quantities are not considered in this study. The X and Y coordinates of the missile impact location (defined as the location of impact of the geometric center of the $2'' \times 4''$ section of the missile) are modeled as uniform random variables. The values of the model parameters represented as deterministic quantities as well as the statistical description of the parameters modeled as random variables are provided in Table 1. Mean values of the aluminum random mechanical properties are obtained from Kaufman, (2008), while the pine wood elastic modulus and mass density are taken from FPL (2010). Due to the lack of statistical information regarding the mechanical properties of 3004H34 aluminum, the types of probability distributions and the coefficients of variation (COVs) are selected based on engineering judgment and information regarding similar metallic materials. All random parameters are modeled as statistically independent random variables.

4. Determination of an appropriate *IM*

PBE applications require the identification of a sufficient and efficient *IM*. In this context, an *IM* is said to be sufficient when it renders the *EDP* independent of other parameters such as missile type and missile mass, while an *IM* is said to be efficient when its use produces a small variance in the *EDP* (Luco and Cornell, 2007). In this study, only scalar quantities directly related to the impact intensity are considered as potential *IM*s. The effects produced by different missile shapes, impact locations, and angles of impact can also be included in the sufficiency study for the *IM*s by considering the use of vector-valued *IM*s (Bazzurro, 1998; Baker and Cornell, 2008). However, identification of the optimal *IM* for the problem at hand, albeit very important, is a very complex problem that is beyond the scope of this paper.

Three possible choices of *IM*s are considered here: (1) the missile impact velocity, V_m, (2) the missile impact linear momentum, LM_m, and (3) the missile impact kinetic energy, KE_m. The choice of these three potential scalar-valued *IM*s is based on existing studies available in the literature, which focus on the use of these three quantities for the evaluation of the performance of storm panels (NAHB, 2002; Borges et al., 2009; Masters et al., 2010). These potential *IM*s are evaluated for sufficiency by using a deterministic FE model for WBD impact analysis, with material parameters set at their mean value and a constant point of impact corresponding to the center of the panel. This model is referred to as the "mean model". Impacts are simulated at various levels of the possible *IM*s, by considering missiles of three different weights, i.e., 9, 12, and 15 pounds (corresponding to masses of 4.08, 5.44, and 6.80 kg), and by varying the velocity of the WBD impacts. The ranges considered in this study for the three potential *IM*s are: (1) $V_m \le 49.5$ m/s, (2) $LM_m \le 260.8$ kg m/s, and (3) $KE_m \le 5.00$ kJ. The results presented hereinafter and the corresponding observations are valid only for the considered ranges of *IM*s.

From each dynamic FE analysis, the values of the following two *EDP*s are recorded: (1) the maximum total deflection of the storm panel during impact, Δ_{max}, and (2) the maximum plastic deflection of the storm panel after impact, Δ_{pl}. The *EDP* values are extracted from the FE model's output database through ABAQUS CAE. Δ_{max} is computed as the maximum displacement in the direction of impact over the entire response time history for all nodes of the panel's FE model. This *EDP* is chosen because it is related to the possible damage to the windows protected by the storm panel. Δ_{pl} is defined as the largest residual displacement after impact in the direction orthogonal to the plane of the panel. This *EDP* is chosen because it is related to the possible damage to the storm panel itself. The values of Δ_{max} and Δ_{pl} recorded for the mean model are denoted as $\Delta^0_{max}$and Δ^0_{pl}, respectively. A typical time history of the deflection of a node of the mean model during the dynamic impact analysis is shown in Fig. 3. This node is chosen as node 15,310, with coordinates $X_{15310}=15.39$ cm and $Y_{15310}=60.33$ cm (i.e., close to the center of the panel). Fig. 3 also shows the values of the total deflection ($\Delta^0_{max,15310}$) and of the plastic deflection ($\Delta^0_{pl,15310}$) for node 15,310.

The *EDP* values for the mean model are plotted versus their corresponding *IM* values in Figs. 4–6 in order to determine the sufficiency of the three potential *IM*s considered in this study. In particular, Fig. 4 plots the *EDP*s as functions of V_m, Fig. 5 plots the *EDP*s as functions of LM_m, and Fig. 6 plots the *EDP*s as functions of KE_m.

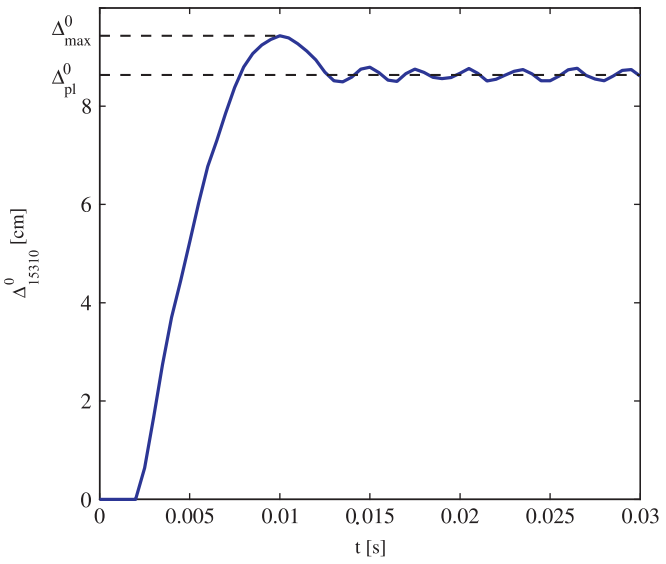

Fig. 3. Typical time history of the nodal deflection along the impact direction (node 15,310).

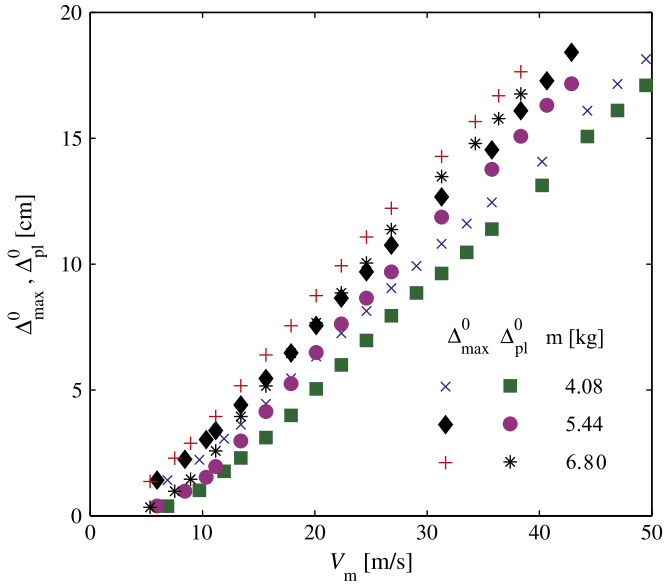

Fig. 4. *EDP*s' values for the mean model considering V_m as *IM*.

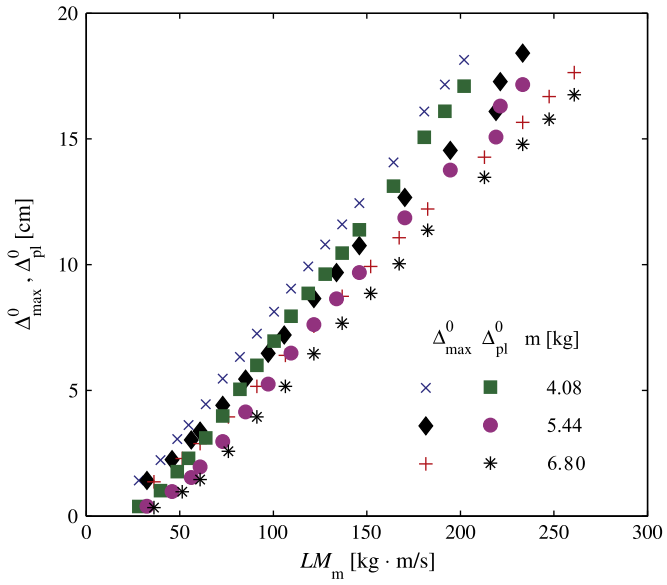

Fig. 5. *EDP*s' values for the mean model considering LM_m as *IM*.

It is observed that both Δ^0_{max} and Δ^0_{pl} present a significant scatter when V_m and LM_m are used as *IM*. In fact, the *EDP*s are dependent on V_m and LM_m (with an approximately linear functional dependency) and on the weight of the missile. In contrast, for values of KE_m smaller than or equal to 3.50 kJ, the values of the two *EDP*s are practically independent of the weight of the missile when KE_m is used as *IM*. Thus, KE_m is identified as the only sufficient *IM* (among the three potential *IM*s considered here) for the *EDP*s considered in this study, at least in the range $KE_m \le 3.50$ kJ. It is found that, for values of KE_m larger than 0.250 kJ, $\Delta^0_{max}$and Δ^0_{pl} can be expressed as quadratic functions of KE_m. The following relations are found by using a least-square fitting procedure for $0.25\ \text{kJ} \le KE_m \le 3.50$ kJ and by adding a quadratic interpolation curve for $0\ \text{kJ} \le KE_m < 0.25$ kJ:

$$\Delta^0_{max} = \begin{cases} -25.345 \times (KE_m)^2 + 18.460 \times KE_m & 0 \le KE_m < 0.25 \\ -0.713 \times (KE_m)^2 + 6.144 \cdot KE_m + 1.540 & 0.25 \le KE_m \le 3.50 \end{cases}$$

$$[\text{units}: \text{cm, kJ}] \quad (3)$$

$$\Delta^0_{pl} = \Delta^0_{max} = \begin{cases} -1.675 \times (KE_m)^2 + 6.903 \times KE_m & 0 \le KE_m < 0.25 \\ -0.745 \times (KE_m)^2 + 6.438 \times KE_m + 0.058 & 0.25 \le KE_m \le 3.50 \end{cases}$$

$$[\text{units}: \text{cm, kJ}] \quad (4)$$

The fitting curves given in Eqs. (3) and (4) are shown in Fig. 6. The quadratic fitting provides a very good representation of the results obtained from the FE analyses. This finding suggests that the *EDP-IM* relations $\Delta^0_{max} - KE_m$ and $\Delta^0_{pl} - KE_m$ can be estimated with sufficient accuracy using only three FE analyses (e.g., for $KE_m = 0.25$ kJ, $KE_m = 1.625$ kJ, and $KE_m = 3.50$ kJ). In the range $3.50\ \text{kJ} < KE_m \le 5.00$ kJ, Δ^0_{max} and Δ^0_{pl} present a larger scatter with respect to the missile mass than for smaller values of KE_m.

The a-posteriori analysis of the maximum strain in the storm panel shows that, for $2.00\ \text{kJ} < KE_m \le 3.50$ kJ, the plastic strain can reach values larger than the strain at rupture in small localized regions of the panel (usually corresponding to the first points of contact between the panel and the corners of the impacting face of the missile). However, for $KE_m > 3.50$ kJ, the plastic strain becomes higher than the aluminum rupture strain in large regions around the impact location. In addition, the a-posteriori analysis of the principal stresses in the wooden missile shows that, for $2.00\ \text{kJ} < KE_m \le 3.50$ kJ, the maximum compressive stresses in the missile become larger than the lower bound for the compressive strength (2.34 ksi = 16.1 MPa) of pine wood under saturated conditions, while the maximum compressive stresses in the missile become larger than the average value of the compressive strength (3.12 ksi = 21.5 MPa) of pine wood under saturated conditions (Green and Kretschmann, 1994). Since the FE model employed in this study does not explicitly model fracture of the aluminum panel and/or fragmentation of the wooden missile, this FE model provides results that are very accurate for $KE_m \le 2.00$ kJ, and accurate for $2.00\ \text{kJ} < KE_m \le 3.50$ kJ. However, the same FE model is not adequate to realistically capture the behavior at impact of the panel-missile system for $KE_m > 3.50$ kJ, due to the modeling limitations described above (i.e., linear elastic missile and non-explicit modeling of fracture in the aluminum panel). Thus, the results presented throughout the remainder of this study are limited to values of the impact kinetic energy $KE_m \le 3.50$ kJ. It is noteworthy that, even with the above limitations, the results of this study can be used to analyze the

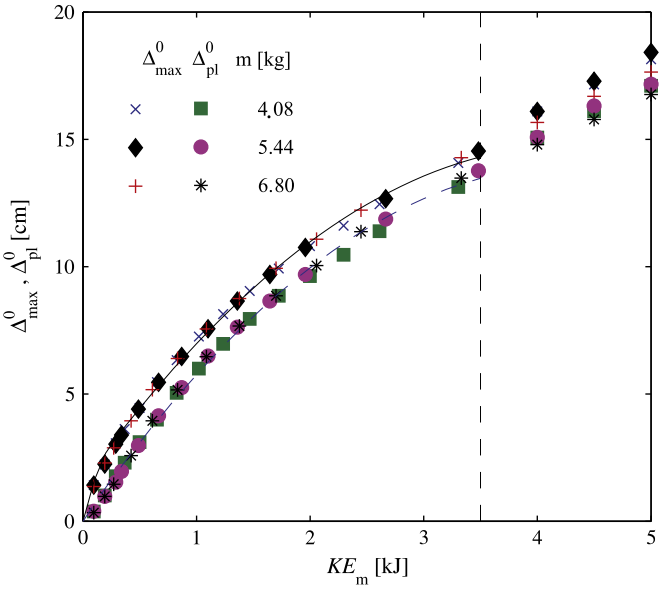

Fig. 6. *EDP*s' values for the mean model considering KE_m as *IM*.

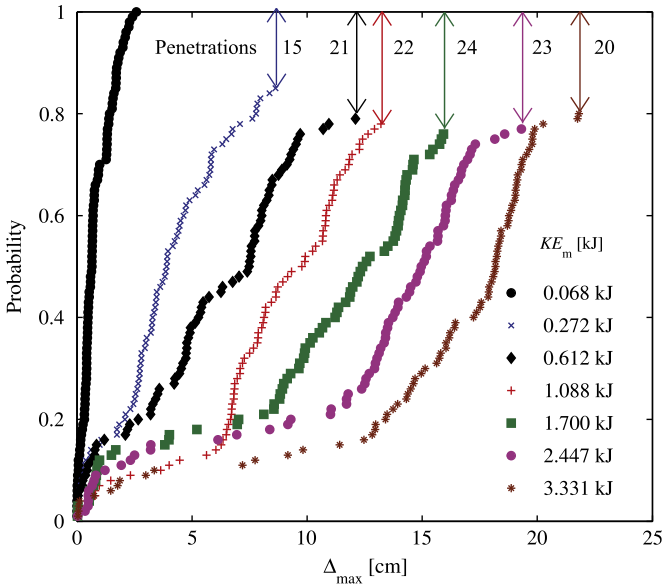

Fig. 7. Empirical CDFs for Δ_{max} including all types of impacts.

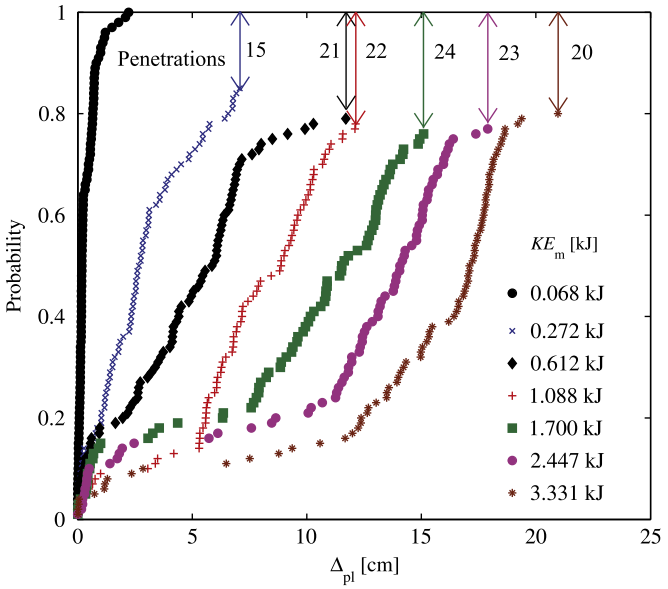

Fig. 8. Empirical CDFs for Δ_{pl} including all types of impacts.

performance of aluminum storm panels under a wide range of realistic conditions corresponding to moderate hurricanes. In fact, $KE_m = 3.50$ kJ corresponds to the kinetic energy of a 9-pound missile impacting the storm panel at a speed of approximately 92.6 mph = 41.4 m/s. Assuming a WBD flight time of $1\text{ s} \le t \le 3\text{ s}$ and using the relations given in Lin et al. (2007) to evaluate the ratio between the WBD speed, V_m, and the 3-s wind gust speed U_w, the 3-s wind gust speed corresponding to $KE_m = 3.50$ kJ is estimated as $50.2\text{ m/s} \le U_w \le 73.0\text{ m/s}$ ($112.3\text{ mph} \le U_w \le 163.3\text{ mph}$).

Based on the results obtained, it is inferred that KE_m is an appropriate *IM* for BECs with ductile behavior, at least for moderate values of KE_m (i.e., for $KE_m \le 3.50$ kJ for the storm panel considered in this study). This result is consistent with results recently made available in the literature (Holmes, 2008). It is noted here that most of the studies currently available in the literature are focused on WBD impact on glass and/or other BECs with brittle behavior and suggest the use of LM_m as *IM* for these types of BECs (NAHB, 2002; Masters et al., 2010).

5. Structural analysis results and statistical characterization of the *EDP*s

In the structural analysis phase, the statistical description of the *EDP*s conditional to the value of the identified *IM* (i.e., KE_m) is obtained by using stochastic FE analysis for the BECs subjected to WBD impact. A statistically representative number of samples of the random parameters are obtained using MCS for each level of *IM*. The sampled values of the parameters are used as input to define the different sample FE models. Based on preliminary FE analyses, a number of 100 simulations per *IM* level is selected in order to identify an appropriate distribution for the fragility curves with an adequate accuracy for engineering applications. The different levels of the *IM* are obtained by using only one missile weight (i.e., 15-pound missile) and by varying the velocity of the missile.

5.1. Identification of impact typologies

Figs. 7 and 8 plot the empirical CDFs for Δ_{max} and Δ_{pl}, respectively, for different levels of KE_m (i.e., $KE_m = 0.068$, 0.272, 0.612, 1.088, 1.700, 2.447, and 3.331 kJ). Each CDF is obtained from the results of 100 stochastic FE analyses at a specific level of *IM*. Three distinct regions can be identified in each of these empirical CDFs.

The first region corresponds to a concentration of FE analyses resulting in very small values of Δ_{max} and Δ_{pl}. The second region includes FE analyses which provide values of Δ_{max} and Δ_{pl} that are more spread out. Finally, the third region in the empirical CDFs corresponds to the FE analyses in which the missile penetrates the storm panel. In this paper, these impacts are referred to as "penetrations". For these FE analyses, it is not possible to identify specific numerical values of Δ_{max} and Δ_{pl}. Thus, similar to a common convention used in PBEE (Vamvatsikos and Cornell, 2002), infinite values are assigned to the *EDP*s corresponding to penetration. The number of penetrations is recorded at each level of *IM*. This number of penetrations is reported in Figs. 7 and 8. It is observed that no penetration is recorded for $KE_m = 0.068$ kJ and that, for $0.612\text{ kJ} \le KE_m \le 3.331$ kJ, the number of penetrations does not vary significantly for different levels of KE_m.

The empirical CDFs shown in Figs. 7 and 8 can be better interpreted by analyzing the WBD impact locations and the corresponding impacts' characteristics. In particular, it is observed that the recorded values of Δ_{max} and Δ_{pl} are usually very small when the impact locations belong to the portion of the storm panel where the fixed boundary conditions are applied (including an additional rectangular area along the short side of the panel of width equal to one half of the height of the $2'' \times 4''$ missile, i.e., 4.45 cm). These impacts are referred to as "boundary impacts" in this paper, since the values of the *EDP*s critically depend on the boundary conditions applied. The main effect of these boundary impacts is a net reduction in the vulnerable area of the panel, assuming that the wall on which the panel is attached is not vulnerable to damage from WBD impact. More generally, the values of the *EDP*s for boundary impacts depend not only on the storm panel's properties, but also on the properties of the structural component on which the storm panel is installed. In contrast, when the impacts do not occur on this portion of the storm panel and are not penetrations, larger values of Δ_{max} and Δ_{pl} are usually recorded. In this paper, these impacts are referred to as "ordinary impacts". Fig. 9 shows the impact locations on the storm panel and the corresponding impact types (i.e., boundary

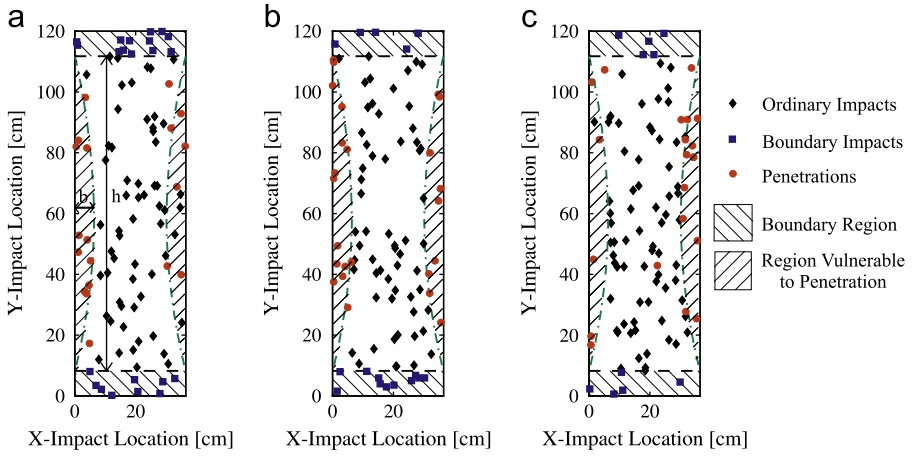

Fig. 9. Impact locations and corresponding impact types: (a) KE_m=0.612 kJ, (b) KE_m=1.700 kJ, and (c) KE_m=3.331 kJ.

impacts, ordinary impacts, and penetrations) of 100 FE analyses with random material properties and random impact locations for 15-pound missiles impacting at 30, 50, and 70 mph (i.e., for KE_m=0.612, 1.700, and 3.331 kJ, respectively).

It is noteworthy that the impact locations of the penetrations are concentrated in the portions of the storm panel which are located near the unconstrained sides. The dimensions of these portions are practically constant for all the values of KE_m, and can be approximately identified with two symmetric parabolic segments with basis b=103.51 cm and height h=6.35 cm (see Fig. 9). The sum of the areas of these two parabolic segments correspond to 20.0% of the area of the panel, which is very close to the average ratio between the number of penetrations and the total number of impact analyses estimated over the range 0.612 kJ $\leq KE_m \leq$ 3.331 kJ (i.e., 22.0%, with 110 penetrations out of 500 FE simulations). Considering the entire range $KE_m \leq$ 3.331 kJ for which FE response analyses are available, 101 of the 125 penetrations recorded are located within these two symmetric parabolic segments. These observations suggest that, for $KE_m \leq$ 3.331 kJ, penetration is dependent on impact location and boundary conditions rather than intensity of the WBD impact and variability of the storm panel's material properties.

5.2. Statistical characterization of the EDPs for ordinary impacts

The variability of the *EDP*s corresponding to ordinary impacts is also of interest. New empirical CDFs are obtained considering only the values of the *EDP*s obtained from the ordinary impacts (i.e., by eliminating the results corresponding to the boundary impacts and the penetrations, and then by normalizing the probability of the remaining results to 1). From these values, the means and standard deviations for Δ_{max} and Δ_{pl} are computed at the different levels of KE_m. The normal, lognormal, and truncated normal (with lower truncations at Δ_{max}=0 cm and Δ_{pl}=0 cm, respectively) distributions are compared in order to find the best fit to the ordinary impacts' results. This comparison is performed by using the modified Kolmogorov–Smirnov goodness-of-fit test (Kececioglu, 1993), which accounts for the fact that the distributions' parameters are estimated from the data. Fig. 10 illustrates the empirical CDF for *EDP* Δ_{max}, and the analytical CDFs corresponding to KE_m equal to 0.612 kJ (i.e., corresponding to 15-pound missiles impacting at 30 mph) for all considered distributions.

In the modified Kolmogorov–Smirnov test, the proposed distribution is accepted at a given significance level, α, if the maximum difference between the empirical CDF and the analytical CDF, D_n, is less than the critical value, $D_{n,\alpha}$, corresponding to the given level of significance (Kececioglu, 1993). If multiple distributions are acceptable at a given significance level, a more detailed statistical analysis (e.g., involving the use of the method of matching moments, maximum likelihood tests, and/or probability plots (Ang and Tang, 1975; Kececioglu, 1993)) is needed to decide the best fit. Table 2 presents the results of the modified Kolmogorov–Smirnov testing on the reduced data sets at a significance levels α=5% and α=1%. The critical $D_{n,\alpha}$ values are

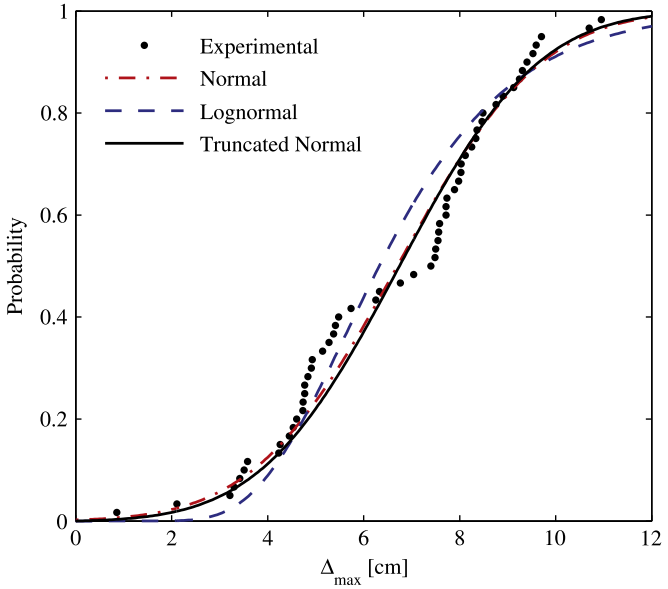

Fig. 10. Empirical and fitted CDFs of Δ_{max} for ordinary impacts and KE_m=0.612 kJ.

Table 2
Modified Kolmogorov–Smirnov test results for the probabilistic characterization of the *EDP*s corresponding to ordinary impacts.

KE_m [kJ]	N	Observed D_n ($\Delta_{max}-\Delta_{pl}$) Distribution			Critical D_n α	
		Normal	Lognormal	Truncated Normal	0.05	0.01
0.068	80	0.219–0.220	0.263–0.225	0.209–0.231	0.106	0.123
0.272	66	0.117–0.160	**0.063–0.100**	**0.078**–0.112	0.109	0.127
0.612	60	0.117–**0.086**	0.178–0.129	**0.114–0.085**	0.114	0.133
1.088	69	0.111–**0.096**	0.132–0.125	0.113–**0.099**	0.107	0.124
1.700	60	**0.113–0.102**	0.135–0.133	0.118–**0.111**	0.114	0.133
2.448	62	**0.074–0.085**	**0.093**–0.122	**0.069–0.084**	0.113	0.131
3.331	70	0.158–0.163	0.188–0.196	0.164–0.160	0.106	0.123

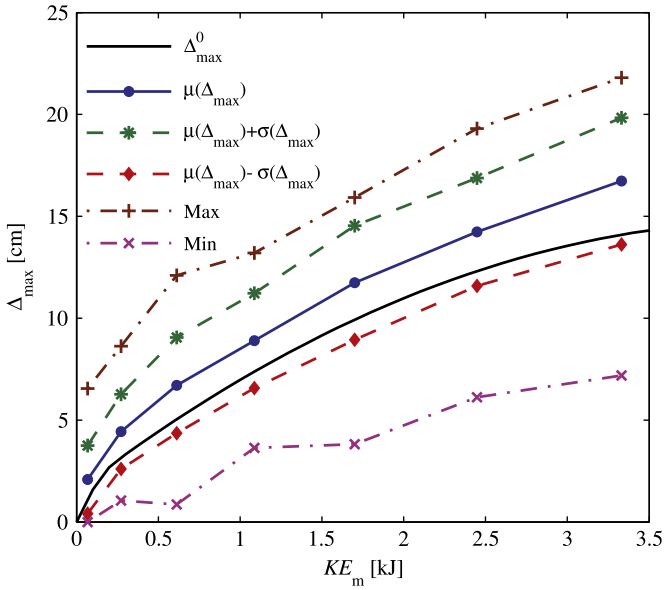

Fig. 11. Comparison of Δ^0_{max} and statistics of Δ_{max}.

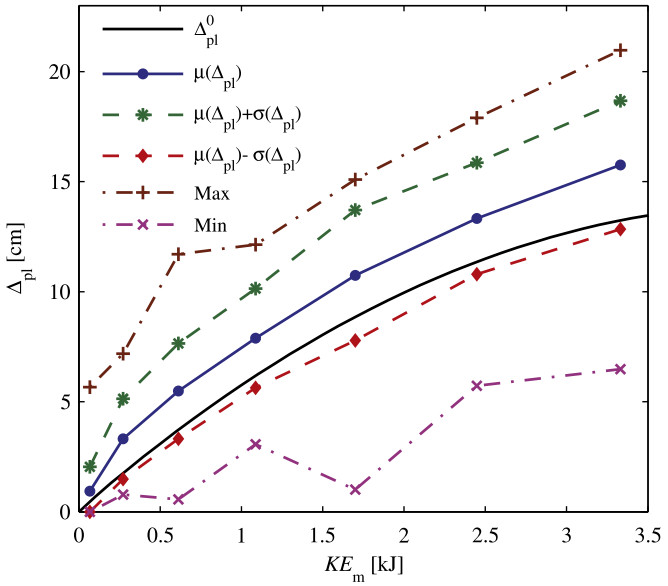

Fig. 12. Comparison of Δ^0_{pl} and statistics of Δ_{pl}.

obtained from Kececioglu (1993). In Table 2, bolded D_n values indicate that the considered probability distribution is acceptable at $\alpha=5\%$ significance, and underlined D_n values indicate that considered probability distribution is acceptable at $\alpha=1\%$ significance.

It is observed that (1) at 5% significance, many of the data sets can be represented by normal or truncated normal distributions, while in only three cases out of 14 a lognormal distribution can be accepted; (2) at 1% significance, a normal or truncated normal distribution is acceptable in most of the cases (with the exception of the largest and smallest value of KE_m for both normal and truncated normal distribution, and of $KE_m=0.272$ kJ and Δ_{pl} for the normal distribution), while a lognormal distribution is acceptable only in two cases out of seven for Δ_{max} and in four cases out of seven for Δ_{pl}; and (3) for $KE_m=0.068$ kJ, none of the considered theoretical distributions are acceptable to describe the data obtained from simulation. Thus, the lognormal distribution is excluded as a possible fit for the data, and the truncated normal distribution is preferred over the normal distribution in the range $0.272\ \text{kJ} \le KE_m \le 2.442\ \text{kJ}$ because it avoids physically impossible negative values of Δ_{max} and Δ_{pl}.

Fig. 11 compares the mean values of Δ_{max}, $\mu(\Delta_{max})$, corresponding to the ordinary impacts in the probabilistic FE model simulations and the Δ^0_{max} curve given in Eq. (2). Fig. 11 also shows the values of $\mu(\Delta_{max})$ plus/minus one standard deviation, $\sigma(\Delta_{max})$, as well as the minimum and maximum values of Δ_{max} recorded over all the FE analyses performed (denoted as "Min" and "Max", respectively, in Fig. 11).

It is observed that the curve $\mu(\Delta_{max})$ is consistently higher than Δ^0_{max}, and the minimum and maximum values of Δ_{max} show a significant asymmetry when compared with the $\mu(\Delta_{max})$ curve (i.e., the difference between the $\mu(\Delta_{max})$ and the Min curve is significantly larger than the difference between the $\mu(\Delta_{max})$ and the Max curve). The standard deviation $\sigma(\Delta_{max})$ increases at a slower rate than $\mu(\Delta_{max})$ as KE_m increases, i.e., the COV (i.e., the ratio $\sigma(\Delta_{max})/\mu(\Delta_{max})$) significantly decreases (from 0.663 to 0.186) in the $0.068\ \text{kJ} \le KE_m \le 3.331\ \text{kJ}$ range. The two curves $\mu(\Delta_{max})-\sigma(\Delta_{max})$ and Δ^0_{max} are close in the same KE_m range. The difference between the mean *EDP* $\mu(\Delta)$ and the *EDP* of the mean model, Δ^0, can be represented as normalized discrepancy $\delta(\Delta)$, defined as

$$\delta(\Delta)=\frac{\mu(\Delta)-\Delta^0}{\sigma(\Delta)} \tag{5}$$

Table 3
Statistics of *EDP*s.

KE_m [kJ]	μ [cm]		σ [cm]		COV [%]		δ [%]	
	Δ_{max}	Δ_{pl}	Δ_{max}	Δ_{pl}	Δ_{max}	Δ_{pl}	Δ_{max}	Δ_{pl}
0.068	2.46	1.09	1.63	1.07	66.3	98.2	81.1	58.7
0.272	4.44	3.31	1.84	1.82	41.4	55.1	69.6	85.3
0.612	6.70	5.48	2.35	2.17	35.0	39.6	71.1	81.2
1.088	8.90	7.89	2.33	2.25	26.2	28.6	65.2	75.8
1.700	11.74	10.74	2.80	2.96	23.8	27.6	64.9	64.1
2.448	14.23	13.33	2.65	2.53	18.6	19.0	72.7	78.1
3.331	16.73	15.76	3.10	2.92	18.6	18.5	84.8	86.5

in which Δ denotes Δ_{max} or Δ_{pl}, and Δ^0 denotes Δ^0_{max} or Δ^0_{pl}. It is observed that $\delta(\Delta_{max})$ assumes values close to about 70% over the range $0.272\ \text{kJ} \le KE_m \le 3.331\ \text{kJ}$ and to about 80% for smaller and larger values of KE_m. The last observation suggests that it may be possible to obtain an approximate estimate of the mean and standard deviation from the Δ^0_{max} curve. Fig. 12 compares the Δ^0_{pl}, $\mu(\Delta_{pl})$, $\mu(\Delta_{pl})+\sigma(\Delta_{pl})$, and $\mu(\Delta_{pl})-\sigma(\Delta_{pl})$ curves, and shows the minimum and maximum values of Δ_{pl} recorded over all the FE analyses performed. Similar observations can be made for Δ_{pl} as those made for Δ_{max} in Fig. 11. In particular, the coefficient of variation $\sigma(\Delta_{pl})/\mu(\Delta_{pl})$ decreases from 0.982 for $KE_m=0.068$ kJ to 0.185 for $KE_m=3.331$ kJ, and the normalized discrepancy $\delta(\Delta_{pl})$ remains close to about 80% over the considered KE_m range, with the exception of the case $KE_m \le 0.068$ kJ, for which $\delta(\Delta_{pl})=58.7\%$. Table 3 reports the values of the mean, standard deviation, COV, and normalized discrepancy for both Δ_{max} and Δ_{pl}.

5.3. Effects of impact location variability and boundary conditions

The effects of the impact location variability and boundary conditions are studied by performing 100 FE analyses for $KE_m=1.088$ kJ (i.e., for a 15-pound missile impacting the panel at 40 mph): (1) with random impact locations (with the same probability distributions as described in Table 1) and the same boundary conditions described in Fig. 2, but with deterministic material parameters (with values set equal to their means, see Table 1); and (2) with random impact locations and material parameters (with the same probability distributions as described in Table 1), but different boundary conditions (see Fig. 13). The

new boundary conditions correspond to the same installation previously considered (i.e., the mounting of the panel on a fixed rail system); however, in this case, the storm panel is wider than the opening required for the window and it overlaps with the installation wall by 0.5 in (1.27 cm) along the two unconstrained sides of the panel. The comparison between the performance of the storm panel using the new and original boundary conditions provides important information regarding the acceptable maximum side clearance for storm panel installations. In fact, the 2010 Florida Building Code (ICC, 2011) allows a maximum side clearance between the shutter and a wall or inset surface up to ¼ in (6.4 mm), and requires end closure or shutter overlap for any wider side clearance. The original boundary conditions correspond to an installation case with a side clearance smaller or equal to ¼ in between the shutter and an inset surface, while the new boundary conditions correspond to an installation case with a side clearance smaller or equal to ¼ between the shutter and a wall (see Fig. 13(b)). The portions of the wall that overlap with the installed panel are explicitly incorporated into the FE model in order to simulate the effects of the contact between the deformed panel subject to WBD impact and the wall. The wall is considered sufficiently strong to tolerate impact without damage (a hypothesis that represents a reasonable approximation for brick and/or concrete walls) and is modeled as a rigid component by constraining all DOFs of the corresponding FE portion. In order to simulate the impact between the deformed panel and the rigid wall, two new surface-to-surface contact pairs are defined between the panel and the new portion of the FE model representing the wall.

Fig. 14 shows the impact points and the corresponding impact type with $KE_m = 1.088$ kJ for the case (1) with random material properties and impact locations and original boundary conditions (referred to as "Original Model") in Fig. 14(a); (2) with random impact locations, deterministic material parameters and original boundary conditions (referred to as "Deterministic Material") in Fig. 14(b); and with random impact locations and material parameters but new boundary conditions (referred to as "New BCs") in Fig. 14(c).

For the Deterministic Material case, 27 penetrations are recorded out of the 100 FE simulations, compared to the 22 penetrations recorded for the Original Model case. 22 of the 27 penetrations (i.e., 81.5%) occur within the two symmetric parabolic segments previously identified as the storm panel's portions that are vulnerable to penetration. For the New BCs case, only four penetrations are recorded out of the 100 FE simulations. This reduction of the number of penetrations is very significant, since it is obtained with a relatively small modification of the boundary conditions which can be easily implemented in practical applications (e.g., by introducing into building codes minimum requirements on the overlap between walls and storm panels). The storm panel's portion where the missile impacts can be classified as boundary impacts (i.e., impacts producing very small deflections due to the boundary conditions in the FE model) is significantly larger when compared to the Original Model case. In fact, in addition to the two regions at the top and at the bottom of the panel identified in the Original Model case, this portion includes two additional regions located along the unconstrained sides of the panel which have a width equal to the width of the overlap between the wall and the storm panel plus one half of the width of the missile (i.e., 3.175 cm). From Fig. 14(c), it is observed that three of the four recorded penetrations in the New BCs case occur within the region defined as the difference between the two symmetric parabolic segments identified as vulnerable to penetration in the Original Model case and the new region with boundary impacts. The impact location of the fourth penetration is also very close to the vulnerable region identified above. The previous observations confirm that, for the range $0.612 \text{ kJ} \le KE_m \le 3.331$ kJ, penetration of storm panels is strongly dependent on the missile's impact location and storm panel's boundary conditions, while it is only weakly dependent on the variability of the storm panel's material properties. In addition, the results presented in this paper suggest that the installation configuration with a side clearance between the storm panel and an inset surface performs significantly worse than other admissible configurations, independent of the size of the side clearance.

Figs. 15 and 16 compare the empirical CDFs of the *EDP*s Δ_{max} and Δ_{pl}, respectively, relative to $KE_m = 1.088$ kJ and corresponding to ordinary impacts for the Original Model, Deterministic Material, and New BCs cases.

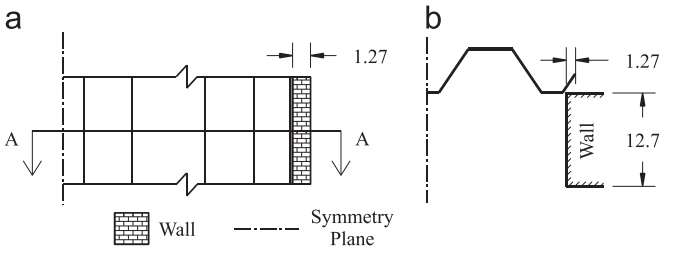

Fig. 13. Boundary conditions corresponding to storm panel wider than window opening (New BCs case (all dimensions in cm)): (a) Front view, and (b) section view.

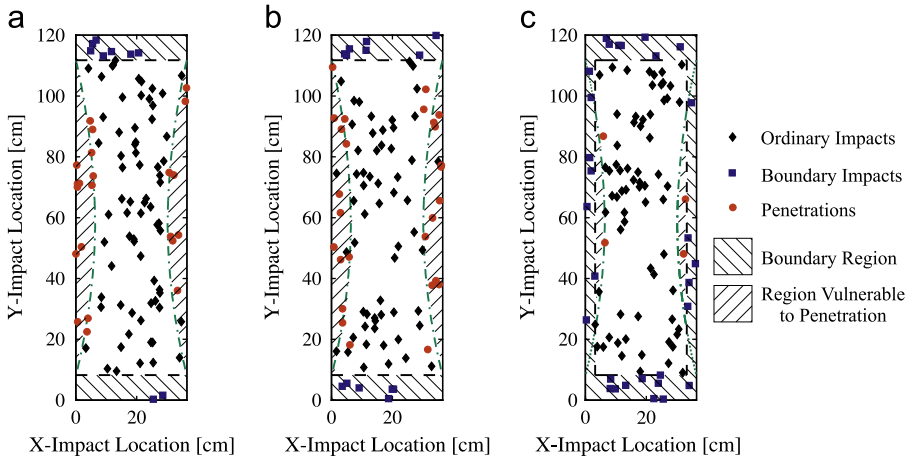

Fig. 14. Impact locations and corresponding impact types for $KE_m = 1.088$ kJ: (a) Original Model case, (b) Deterministic Material case, and (c) New BCs case.

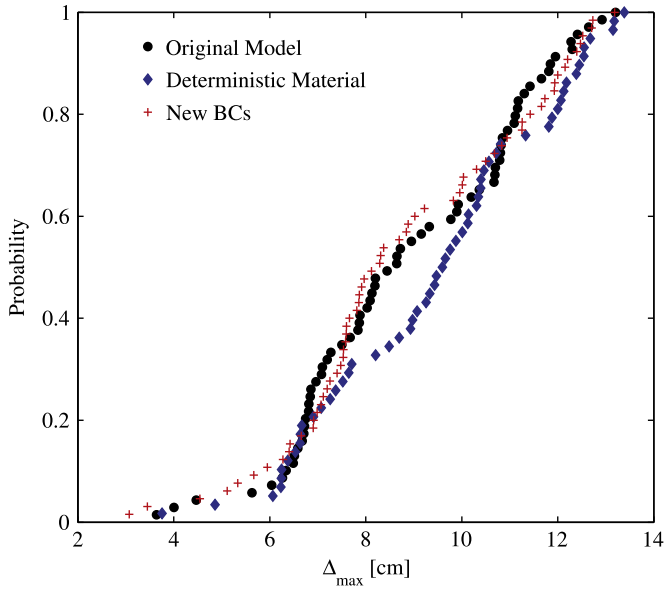

Fig. 15. Effects of boundary conditions and material variability on the empirical CDFs of Δ_{max} for ordinary impacts and KE_m=1.088 kJ.

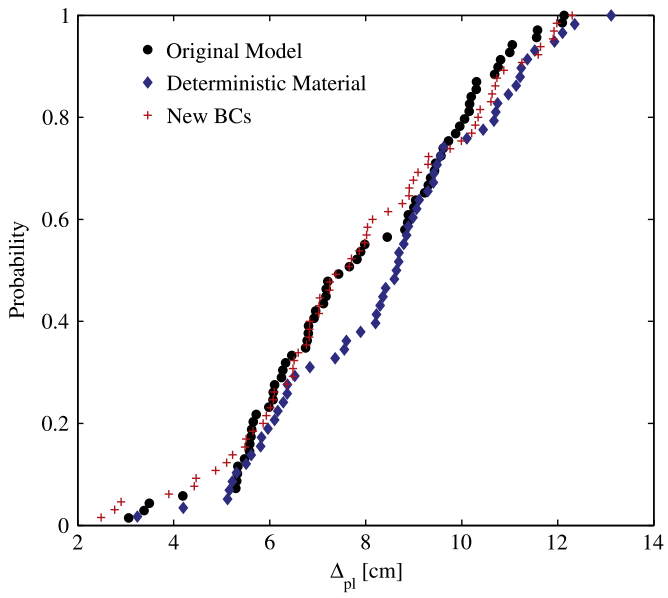

Fig. 16. Effects of boundary conditions and material variability on the empirical CDFs of Δ_{pl} for ordinary impacts and KE_m=1.088 kJ.

In both Figs. 15 and 16, the three empirical CDFs are similar, particularly the ones corresponding to the Original Model and the New BCs cases. The CDFs of Δ_{max} and Δ_{pl} corresponding to the Deterministic Material case have a slightly smaller mean than the other two cases. These results suggest that, in contrast to the number of penetrations and boundary impacts, the variability of the material parameters has a greater influence (albeit overall small) than the boundary conditions on the probability distributions of the *EDP*s relative to ordinary impacts only.

6. Damage analysis results and development of fragility curves

In the damage analysis phase, the *EDP*s (Δ_{max} and Δ_{pl}) obtained in the structural analysis phase are compared to relevant *DM*s, including a measure of damage to the panel itself, a measure of damage to the window behind the panel, and a measure of complete penetration. Following a procedure commonly used in PBEE, the physical damage conditions are represented using a limit state function g for each damage limit state, i.e.,

$$g = DM_{lim} - EDP \quad (6)$$

where DM_{lim} denotes the limit state capacity (also called failure threshold). According to this procedure, the physical damage is described using discrete limit states instead of continuous *DM*s, and failure with respect to a given damage state is reached when $g \le 0$, or (equivalently) when $EDP \ge DM_{lim}$. It is noted here that the term "failure" does not necessarily represent the physical failure of the storm panel, but simply denotes the outcrossing of a specified limit state. Fig. 17 graphically represents the damage limit states considered in this study.

Fig. 17(a) illustrates the limit state corresponding to failure of the panel only. In this scenario, a WBD impact causes the hurricane panel to reach an excessive plastic deformation (i.e., the plastic deformation is enough to render the panel unusable in future storms, yet the maximum deflection of the panel is not enough to damage the window behind it). This failure occurs when the value of the *EDP* Δ_{pl} recorded from the FE model output is larger than or equal to the limit state capacity ξ_{pl} assumed to warrant replacement of the panel (i.e., $\Delta_{pl} \ge \xi_{pl}$). In this study, it is assumed that the ξ_{pl} can be represented as a lognormally distributed random variable with mean $\mu(\xi_{pl})$=2.5 in. (6.35 cm), and coefficient of variation COV(ξ_{pl})=0.10. Fig. 17(b) illustrates the limit state corresponding to excessive deformation of the panel resulting in the failure of both the panel and the window behind it. In this case, a failure occurs when the *EDP* Δ_{max} obtained from the FE analysis is larger than or equal to the limit state capacity ξ_{max}, defined as the minimum distance between the storm panel and the window protected by the panel (i.e., $\Delta_{max} \ge \xi_{max}$). It is assumed that the ξ_{max} can be represented as a lognormally distributed random variable with mean $\mu(\xi_{max})$=5.0 in. (12.70 cm), and coefficient of variation COV(ξ_{max})=0.15. The statistics of ξ_{pl} and ξ_{max} adopted in this paper represent realistic values of the means and COVs based on engineering judgment. However, for real-world applications, these statistics should be obtained from statistical data regarding window installation in the hurricane prone region of interest. Fig. 17(c) illustrates the complete penetration of the panel and window after WBD impact. A simulation corresponding to a missile penetration is also considered a failure with respect to the other two limit states of interest.

Fragility curves are constructed from the data by plotting the probability of failure relative to each limit state versus its corresponding level of *IM*. These curves represent the CDFs of the relevant limit state as functions of KE_m and are presented in Fig. 18.

Each data point in Fig. 18 is representative of 100 stochastic FE simulations at a specific level of the *IM*. Therefore, the probability of failure with respect to each limit state is the number of total failures divided by 100 (i.e., the number of total trials for each discrete KE_m level). In addition to the fragility curves obtained by modeling both ξ_{pl} and ξ_{max} as random variables (referred to as random threshold (RT) fragility curves), Fig. 18 plots the fragility curves obtained by assuming ξ_{pl} and ξ_{max} equal to their mean values (referred to as deterministic threshold (DT) fragility curves). Fig. 18 also provides the confidence interval of $\pm$ one standard deviation for the fragility curve corresponding to the limit state of penetration.

In Fig. 18, it is observed that (1) the DT and RT fragility curves for the *DM* related to the panel failure (i.e., for the limit state $\Delta_{pl} \ge \xi_{pl}$) are extremely close; (2) the RT fragility curve for the *DM* related to the window failure (i.e., for the limit state $\Delta_{max} \ge \xi_{max}$) is significantly flatter (i.e., it is characterized by a larger

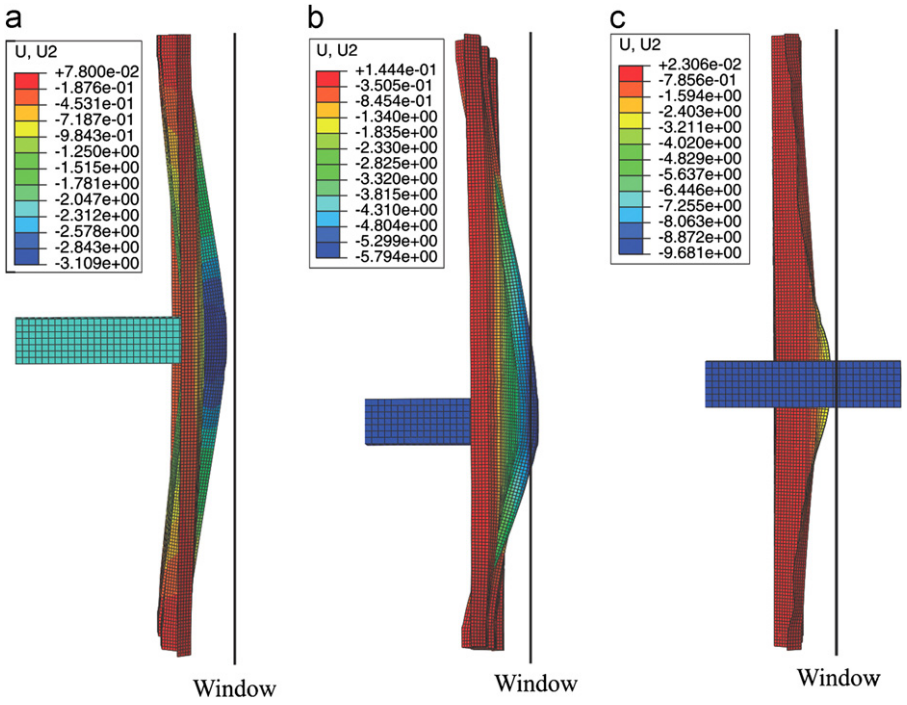

Fig. 17. Damage limit states: (a) Damage to the storm panel, (b) damage to the window, and (c) penetration of the missile.

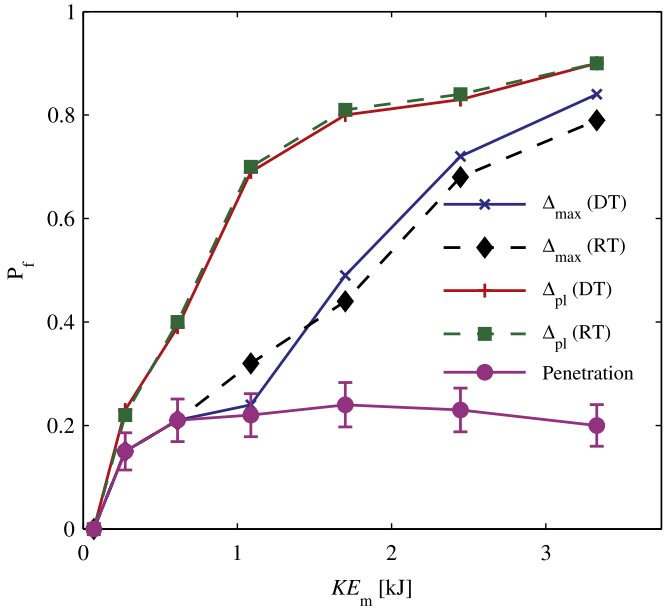

Fig. 18. Fragility curves for hurricane protection panels.

dispersion) than the corresponding DT fragility curve; and (3) for low values of KE_m (i.e., $KE_m \leq 0.612$ kJ), penetrations are the dominant failure condition. Thus, while the panel failure is practically insensitive to the randomness of the limit state capacity, the window failure condition shows a non-negligible dependence on the variability of the limit state capacity.

It is also observed that the values of the failure probability estimates for the penetration limit state do not monotonically increase with KE_m. This phenomenon contrasts with the definition of a fragility curve. However, for this limit state, the standard deviation of the failure probability estimator (which is a measure of the simulation accuracy) is quite large (i.e., slightly more than 4% over the range 0.612 kJ $\leq KE_m \leq$ 3.331 kJ). This result indicates that the limited number of samples used in this study (i.e., 100 samples) introduces a small but not negligible bias in the estimation of the fragility curve for the penetration limit state. For future studies, it is suggested that more accurate estimates of this fragility curve should be obtained by increasing the number of samples used in the MCS, or by adopting variance reduction simulation techniques such as importance sampling (Melchers, 1999).

7. Conclusions

This paper presents the development of windborne debris (WBD) impact fragility curves for building envelope components (BECs) in the context of a performance-based engineering (PBE) methodology for assessment and mitigation of WBD impact hazard produced by hurricanes. These fragility curves provide the probabilistic description of the impact resistance of BECs subject to an impact event described by an appropriate intensity measure (*IM*). Monte Carlo simulation is used in combination with the finite element (FE) method to propagate the uncertainties from modeling parameters (such as material constitutive parameters and impact location) to engineering demand parameters (*EDP*s), i.e., response parameters computed, in this case, by using dynamic impact analysis of nonlinear FE models of BECs and wooden missiles. Appropriate damage measures (*DM*s) are defined to describe relevant physical states of damage and evaluate the structural performance.

This paper focuses on BECs with ductile behavior subjected to the impact of rod-type WBD. For this typology of BECs (which includes the aluminum storm panels for window protection used as an application example in this paper) and rod-type WBD, it is found that the impact kinetic energy, KE_m, is a sufficient *IM* in the range $KE_m \leq 3.50$ kJ. Three damage states are identified, namely (1) damage to the storm panel (with *EDP* corresponding to the maximum plastic deformation of the panel, Δ_{pl}); (2) damage to the window protected by the storm panel (with *EDP* corresponding to the maximum total deflection of the panel, Δ_{max}); and (3) penetration of the panel by the missile. Three typologies of

impacts are identified: (1) boundary impacts (i.e., impacts whose effects are mainly dependent on the installation details of the storm panel and on the strength of the wall on which the panel is installed); (2) penetrations; and (3) ordinary impacts. For boundary impacts, the values of the *EDP*s are generally very small and, under the assumption that the wall is sufficiently resistant to damage from WBD impact, correspond to no building damage. For penetrations, the values of the *EDP*s are infinite and the level of damage to the building is the highest produced by WBD impact. For ordinary impacts, the values of the *EDP*s related to panel damage and window damage show a significant variability and can be described using, e.g., a truncated normal probability distribution. It is observed that impact location has a crucial effect on determining the type of impact and the corresponding damage to the structure. For the range of KE_m considered in this study (i.e., $KE_m \leq 3.50$ kJ), it is also shown that, while boundary impacts and penetrations depend mainly on the boundary conditions (i.e., installation details) of the storm panel, the values of the *EDP*s obtained from ordinary impacts show a small but not insignificant dependency on material variability.

The FE model adopted in this study can model the missile's impact on the storm panel with high accuracy for $KE_m \leq 2.00$ kJ, and with sufficient accuracy for 2.00 kJ $< KE_m \leq 3.50$ kJ. At higher levels of impact kinetic energy, phenomena such as fracture of the aluminum panel and/or fragmentation of the wooden missile start to take place. These phenomena can significantly influence the performance of the storm panels subject to WBD impact. Thus, for $KE_m > 3.50$ kJ, the construction of fragility curves for storm panels requires the development of a FE model that is more advanced than the model employed in this study. This model should be able to explicitly model the fracture of the aluminum panel and/or the fragmentation of the wooden missile.

Development of fragility curves for BECs plays an integral role in the development of a probabilistic performance-based hurricane engineering framework. The procedure developed in this paper can be extended to any type of BEC subject to any type of WBD impacts. Further research is needed to identify appropriate *IM*s, *EDP*s, and *DM*s for different typologies of BECs and structural components of structural systems located in hurricane-prone regions. The effects of a variable angle of WBD impact should be included in the construction of fragility curves. Analytical, numerical, and experimental studies are also needed to extend the results presented in this paper, and to derive the fragility curves corresponding to the impact of compact-type and sheet-type WBD on different BECs.

Acknowledgments

The authors gratefully acknowledge support of this research by (1) the Louisiana Board of Regents (LA BoR) through the Pilot Funding for New Research (Pfund) Program of the National Science Foundation (NSF) Experimental Program to Stimulate Competitive Research (EPSCoR) under Award No. LEQSF(2011)-PFUND-225; (2) the LA BoR through the Louisiana Board of Regents Research and Development Program, Research Competitiveness (RCS) subprogram, under Award No. LESQSF(2010-13)-RD-A-01; (3) the Longwell's Family Foundation through the Fund for Innovation in Engineering Research (FIER) Program; and (4) the LSU Council on Research through the 2009–2010 Faculty Research Grant Program. Any opinions, findings, conclusions or recommendations expressed in this publication are those of the authors and do not necessarily reflect the views of the sponsors. The authors are very thankful to the anonymous reviewers for their constructive criticism of the paper. The reviewers' insightful comments were extremely useful in further improving the original manuscript. The authors would also like to acknowledge Mr. Brian Smoorenburg for his help in extracting the data needed for post-processing from the finite element analysis results.

References

Abu-Farsakh M.Y., Yu X., Yoon S., Tsai C., 2010. Calibration of Resistance Factors Needed in the LRFD Design of Drilled Shafts. Technical Report no. FHWA/LA.10/470.

A.G.I. Group, 2006. Storm panels—architectural and engineering drawings. Last modified March 2011. 〈http://www.stormshutters.com/storm-panels/drawings.html〉 (accessed March 10, 2011).

Ang, A.H.-S., Tang, W.H., 1975. Probability Concepts in Engineering Planning and Design, Volume 1. John Wiley & Sons, Inc., New York, NY, USA.

American Society for Testing and Materials (ASTM), 2005a. Standard E1886: Standard Test Method for Performance of Exterior Windows, Curtain Walls, Doors, and Impact Protective Systems Impacted by Missile(s) and Exposed to Cyclic Pressure Differentials. ASTM International, West Conshohocken, Pennsylvania, USA.

American Society for Testing and Materials (ASTM), 2005b. Standard E1996: Standard Specification for Performance of Exterior Windows, Curtain Walls, Doors and Impact Protective Systems Impacted by Windborne Debris in Hurricanes. ASTM International, West Conshohocken, Pennsylvania, USA.

Augusti, G., Ciampoli, M., 2006. First Steps Towards Performance-based Wind Engineering, Performance of Wind Exposed Structures: Results of the PERBACCO Project. Firenze University Press, Florence, Italy.

Baker, J.W., Cornell, C.A., 2005. A vector-valued ground motion intensity measure consisting of spectral acceleration and epsilon. Earthquake Engineering & Structural Dynamics 34 (10), 1193–1217.

Baker, J.W., Cornell, C.A., 2008. Vector valued intensity measures incorporating spectral shape for prediction of structural response. Journal of Earthquake Engineering 12 (4), 534–554.

Barbato M., Petrini F., Ciampoli M., 2011. A preliminary proposal for a probabilistic performance-based hurricane engineering framework. Proceedings, ASCE Structures Congress, Las Vegas, Nevada, USA; April 14–16, 2011.

Bazzurro P., 1998. Probabilistic seismic demand analysis. Ph.D. Dissertation, Department of Civil and Environmental Engineering, Stanford University, Palo Alto, California, USA.

Belytschko, T., Liu, W.K., Moran, B., 2000. Nonlinear Finite Elements for Continua and Structures. John Wiley & Sons Ltd., West Sussex, England.

Bertero, R.D., Vitelmo, V., 2002. Performance-based seismic engineering: the need for a reliable conceptual comprehensive approach. Earthquake Engineering & Structural Dynamics 31 (3), 627–652.

Borges A., Lopez R.R., Godoy L.A., Lopez R.E.Z., 2009. Impact of windborne debris on storm shutters. Proceedings, 11th Americas Conference on Wind Engineering. San Juan, Puerto Rico, USA; June 22–26, 2009.

Brandenberg, S.J., Zhang, J., Kashighandi, P., Huo, Y., Zhao, M., 2011. Demand Fragility Surfaces for Bridges in Liquefied and Laterally Spreading Ground. PEER Center. University of California, Berkeley, California, USA.

Ciampoli M., Petrini F., Augusti G., 2009. A procedure for performance-based wind engineering. Proceedings, International Conference on Structural Safety and Reliability, Osaka, Japan; September 13–17, 2009.

Cornell, C.A., Krawinkler, H., 2000. Progress and challenges in seismic performance assessment. PEER Center News 3 (2), 1–4.

Dassault Systemes Simulia (DSS), 2008. ABAQUS Standard and Explicit User's Manuals, Version 6.8. Dassault Systemes Simulia Corp., Providence, Rhode Island, USA.

Der Kiureghian, A., Liu, P.L., 1986. Multivariate distribution models with prescribed marginals and covariances. Probabilistic Engineering Mechanics 1 (2), 105–112.

Federal Emergency Management Administration (FEMA), 2007. Multi-hazard estimation methodology—hurricane model. HAZUS-MH-MR4 Technical Manual. 〈www.fema.gov/plan/prevent/hazus/hz_manuals〉 (August 8, 2011).

Fernandez, G., Masters, F.J., Gurley, K.R., 2010. Performance of hurricane shutters under impact by roof tiles. Engineering Structures 32, 3384–3393.

Forest Products Laboratory (FPL), 2010. Wood Handbook—Wood as an Engineering Material. Department of Agriculture, Forest Service, Forest Products Laboratory, General Technical Report FPL-GTR-190, Madison, Wisconsin, USA.

Gardoni, P., Der Kiureghian, A., Mosalam, K.M., 2002. Probabilistic Models and Fragility Estimates for Bridge Components and Systems. PEER Center, University of California, Berkeley, California, USA.

Green, D.W., Kretschmann, D.E., 1994. Moisture Content and the Properties of Clear Southern Pine. Res. Pap. FPL-RP-531. Department of Agriculture, Forest Service. Forest Products Laboratory, Madison, Wisconsin, USA.

Gurley, K., Pinelli, J.P., Subramanian, C., Cope, A.D., Zhang, L., Murphree, J., Artiles, A., Misra, P., Culati, S., Simiu, E., 2005a. Florida Public Hurricane Loss Projection Model. Engineering Team Final Report, Volume I: Exposure and Vulnerability Components of the Florida Public Hurricane Loss Projection Model. Technical Report. International Hurricane Research Center, Florida International University, Miami, Florida, USA.

Gurley K., Pinelli J.P., Subramanian C., Cope A.D., Zhang L., Murphree J., Artiles A., Misra P., Culati S., Simiu E., 2005b. Florida Public Hurricane Loss Projection Model. Engineering Team Final Report, Volume II: Predicting the Vulnerability of Typical Residential Buildings to Hurricane Damage, Technical Report,

International Hurricane Research Center, Florida International University, Miami, Florida, USA.
Gurley K., Pinelli J.-P., Subramanian C., Cope A.D., Zhang L., Murphree J., Arnoldo A., Pranay M., 2006. Florida Public Hurricane Loss Projection Model. Engineering Team Final Report, Volume III: Development Calibration and Validation of Vulnerability Matrices of the Florida Public Hurricane Loss Projection Model. Technical Report, International Hurricane Research Center, Florida International University, Miami, Florida, USA.
Hamburger R.O., Whittaker A.S., 2003. Considerations in performance-based blast resistant design of steel structures. Proceedings, AISC-SINY Symposium on Resisting Blast and Progressive Collapse. American Institute of Steel Construction, New York, NY, USA.
Holmes J., 2008. Windborne debris and damage risk models: a review. Proceedings, Advances in Wind and Structures Conference, Jeju, Korea; May 29–31, 2008.
Holmes, J.D., 2010. Windborne debris and damage risk models: a review. Wind and Structures 13 (2), 95–108.
Hooputra, H., Gese, H., Dell, H., Werner, H., 2004. A comprehensive failure model for crashworthiness simulation of aluminium extrusions. International Journal of Crashworthiness 9 (5), 449–463.
Hossain Q., Mensing R., Savy J., Kimball J., 1999. A probabilistic tornado wind hazard model for the continental United States. Proceedings of the Joint Meeting of the U.S.-Japan Cooperative Program in Natural Resources Panel on Wind and Seismic Effects, 31, 86–92.
Hughes, T.J.R., 1987. The Finite Element Method. Linear Static and Dynamic Finite Element Analysis. Prentice-Hall, Englewood Cliffs, New Jersey, USA.
International Code Council (ICC), 2011. 2010 Florida Building Code, Building. International Code Council, Inc, Washington, DC, USA.
Kakimpa, B., Hargreaves, D.M., Owen, U.S., Martinez-Vazquez, P., Baker, C.J., Sterling, M., Quinn, A.D., 2010. CFD modelling of free-flight and auto-rotation of plate type debris. Wind and Structures 13 (2), 169–189.
Kaufman, J.G., 2008. Properties of Aluminum Alloys. ASM International, Materials Park, Ohio, USA.
Kececioglu, D., 1993. Reliability and Life Testing Handbook, Volume 1. Prentice Hall, Englewood Cliffs, New Jersey, USA.
Kentang, L., 2000. An analysis of the recent severe storm surge disaster events in China. Natural Hazards 21 (2), 215–223.
Kordi, B., Traczuk, G., Kopp, G.A., 2010. Effects of wind direction on the flight trajectories of roof sheathing panels under high wind. Wind and Structures 13 (2), 145–168.
Kwon, O., Kim, E., Orton, S., 2011. Calibration of the live load factor in LRFD bridge design specifications based on state-specific traffic environments. Journal of Bridge Engineering 16 (6), 812–819.
Laursen, T.A., 2002. Computational Contact and Impact Mechanics: Fundamentals of Modeling Interfacial Phenomena in Nonlinear Finite Element Analysis. Springer-Verlag, Berlin, Germany.
Li, Y., Ellingwood, B., 2006. Hurricane damage to residential construction in the US: importance of uncertainty modeling in risk assessment. Engineering Structures 28 (7), 1009–1018.
Lin, N., Letchford, C.W., Holmes, J.D., 2006. Investigations of plate-type windborne debris. I. Experiments in full scale and wind tunnel. Journal of Wind Engineering and Industrial Aerodynamics 94 (2), 51–76.
Lin, N., Holmes, J.D., Letchford, C.W., 2007. Trajectories of windborne debris and applications to impact testing. Journal of Structural Engineering 133 (2), 274–282.
Lin, N., Vanmarcke, E., 2010. Windborne debris risk analysis—Part I. Introduction and methodology. Wind and Structures 13 (2), 191–206.
Lin, N., Vanmarcke, E., Yau, S.-C., 2010. Windborne debris risk analysis—Part II. Application to structural vulnerability modeling. Wind and Structures 13 (2), 207–222.
Liu, J.S., 2001. Monte Carlo Strategies in Scientific Computing. Springer-Verlag, New York, NY, USA.
Lopez, C., Masters, F.J., Bolton, S., 2011. Water penetration resistance of residential window and wall systems subjected to steady and unsteady wind loading. Building and Environment 46 (7), 1329–1342.
Luco, N., Cornell, C.A., 2007. Structure-specific scalar intensity measures for near-source and ordinary earthquake ground motions. Earthquake Spectra 23 (2), 357–392.
Lupoi, G., Franchin, P., Lupoi, A., Pinto, P., 2006. Seismic fragility analysis of structural systems. Journal of Engineering Mechanics 132 (4), 385–395.
Mackie K., Stojadinovic B., 2004. Fragility curves for reinforced concrete highway overpass bridges. Proceedings, 13th World Conference on Earthquake Engineering, Vancouver, Canada; August 1–6, 2004.
Martinez-Vazquez, P., Baker, C.J., Sterling, M., Quinn, A., Richards, P.J., 2010. Aerodynamic forces on fixed and rotating plate. Wind and Structures 13 (2), 127–144.
Masters, F.J., Gurley, K.R., Shah, N., Fernandez, G., 2010. The vulnerability of residential window glass to lightweight windborne debris. Engineering Structures 32 (4), 911–921.
McDonald, J., 1990. Impact resistance of common building materials to tornado missiles. Journal of Wind Engineering and Industrial Aerodynamics 36 (1–3), 717–723.
Melchers, R.E., 1999. Structural Reliability Analysis and Predictions, second ed. Wiley, Chichester, UK.
Minor, J., Harris, P., Beason, W., 1978. Designing for windborne missiles in urban areas. Journal of the Structural Division 104 (11), 1749–1760.
National Association of Home Builders (NAHB) Research Center, 1993. Assessment of Damage to Single-family Homes Caused by Hurricanes Andrew and Iniki. U.S. Department of Housing and Urban Development, Office of Policy Development and Research, Cooperative Agreement H-21172CA, Washington, D.C., USA.
National Association of Home Builders (NAHB) Research Center, 2002. Wind-borne Debris Impact Resistance of Residential Glazing. U.S. Department of Housing and Urban Development, Office of Policy Development and Research, Cooperative Agreement H-21172CA, Washington, D.C., USA.
National Science Board (NSB), 2007. Hurricane Warning: The Critical Need for a National Hurricane Research Initiative. NSB-06-115. National Science Foundation, Arlington, Virginia, USA.
Nowak, A.S., 1999. Report 368. Calibration of LRFD Bridge Design Code. Transportation Research Board, Washington, D.C., USA.
Petrini F., 2009. A Probabilistic Approach to Performance-based Wind Engineering (PBWE). Ph.D. Dissertation, University of Rome "La Sapienza", Rome, Italy.
Pielke, R.A., Gratz, J., Landsea, C.W., Collins, D., Saunders, M.A., Musulin, R., 2008. Normalized hurricane damage in the United States: 1900–2005. Natural Hazards Review 9 (1), 29–42.
Pinelli, J.-P., Simiu, E., Gurley, K., Subramanian, C., Zhang, L., Cope, A.D., Filliben, J., Hamid, S., 2004. Hurricane damage prediction model for residential structures. Journal of Structural Engineering 130 (11), 1685–1691.
Porter K., 2003. An overview of PEER's performance-based earthquake engineering methodology. Proceedings, Conference on Applications of Statistics and Probability in Civil Engineering, San Francisco, California, USA; July 6–9, 2003.
Rini D., Lamont S., 2008. Performance based structural fire engineering for modern building design. Proceedings, Structures Congress, Vancouver, Canada; April 24–26, 2008.
Roeder, B.A., Sun, C.T., 2001. Dynamic penetration of alumina/aluminum laminates: experiments and modeling. International Journal of Impact Engineering 25 (2), 169–185.
Scarabino, A., Giacopinelli, P., 2010. Analysis of the two dimensional sheet debris flight equations: initial and final state. Wind and Structures 13 (2), 109–126.
Shome, N.C., Cornell, C.A., Bazzurro, P., Caraballo, E.J., 1998. Earthquakes, records, and nonlinear responses. Earthquake Spectra 14 (3), 469–500.
Stewart, M.J., 2003. Cyclone damage and temporal changes to building vulnerability and economic risks for residential construction. Journal of Wind Engineering and Industrial Aerodynamics 91 (5), 671–691.
Tachikawa, M., 1983. Trajectories of flat plates in uniform flow with application to wind-generated missiles. Journal of Wind Engineering and Industrial Aerodynamics 14 (1-3), 443–453.
Tachikawa, M., 1988. A method for estimating the distribution range of trajectories of wind-borne missiles. Journal of Wind Engineering and Industrial Aerodynamics 29 (1-3), 175–184.
Twisdale, L., Vickery, P., Steckley, A., 1996. Analysis of Hurricane Windborne Debris Impact Risk for Residential Structures. Technical Report. Applied Research Associates, Inc, Raleigh, North Carolina, USA.
Vamvatsikos, D., Cornell, C.A., 2002. Incremental dynamic analysis. Earthquake Engineering and Structural Dynamics 31 (3), 491–514.
Vamvatsikos, D., Cornell, C.A., 2005. Developing efficient scalar and vector intensity measures for IDA capacity estimation by incorporating elastic spectral shape information. Earthquake Engineering and Structural Dynamics 34 (13), 1573–1600.
Vickery, P.J., Twinsdale, L.A., 1995. Wind-field and filling models for hurricane wind-speed predictions. Journal of Structural Engineering 121 (11), 1700–1709.
Vickery, P.J., Lin, J., Skerlj, P.F., Twinsdale, L.A., Huang, K., 2006. HAZUS-MH Hurricane model methodology. I: Hurricane hazard, terrain and wind load modeling. Natural Hazard Review 7 (2), 82–93.
Vickery, P.J., Masters, F.J., Powell, M.D., Wadhera, D., 2009. Hurricane hazard modelling: the past, present and future. Journal of Wind Engineering and Industrial Aerodynamics 97 (7–8), 392–405.
Willis, J.A.B., Lee, B.E., Wyatt, T.A., 2002. A model of windborne debris damage. Journal of Wind Engineering and Industrial Aerodynamics 90 (4–5), 555–565.
Yau S.C., 2011. Wind Hazard Risk Assessment and Management for Structures. Ph.D. Dissertation, Department of Civil and Environmental Engineering, Princeton University, Princeton, New Jersey, USA.